

# ReadNet: Towards Accurate ReID with Limited and Noisy Samples

Yitian Li, Ruini Xue, Mengmeng Zhu, Qing Xu, and Zenglin Xu

University of Electronic Science and Technology of China  
liyitian1001@gmail.com, xueruini@gmail.com, zmmeng96@163.com,  
xujing.may@gmail.com, zenglin@gmail.com

**Abstract.** Person re-identification (ReID) is an essential cross-camera retrieval task to identify pedestrians. However, the photo number of each pedestrian usually differs drastically, and thus the data limitation and imbalance problem hinders the prediction accuracy greatly. Additionally, in real-world applications, pedestrian images are captured by different surveillance cameras, so the noisy camera related information, such as the lights, perspectives and resolutions, result in inevitable domain gaps for ReID algorithms. These challenges bring difficulties to current deep learning methods with triplet loss for coping with such problems. To address these challenges, this paper proposes READNET, an adversarial camera network (ACN) with an angular triplet loss (ATL). In detail, ATL focuses on learning the angular distance among different identities to mitigate the effect of data imbalance, and guarantees a linear decision boundary as well, while ACN takes the camera discriminator as a game opponent of feature extractor to filter camera related information to bridge the multi-camera gaps. READNET is designed to be flexible so that either ATL or ACN can be deployed independently or simultaneously. The experiment results on various benchmark datasets have shown that READNET can deliver better prediction performance than current state-of-the-art methods.

**Keywords:** Person re-identification, Triplet loss, Adversarial network

## 1 Introduction

Person re-identification (ReID) is a task of identifying bounding boxes of persons in the photos taken by multiple non-overlapping cameras. Given a query image, ReID needs to find out the images of the same ID as the query one. That is, all images of the same person should be retrieved. ReID has been widely adopted in many computer vision applications, such as monitoring, activity analysis, and people tracking [1], so it is critical to design a robust and efficient ReID algorithm.

Due to the high discriminative ability of deep-learned representations, much significant progress of ReID has been made [2–8]. Lots of research considers ReID as a classification problem by taking the person IDs as different classes,

uses softmax loss function to differentiate identities, and learns the feature representations [2–4, 8]. In contrast, some others directly leverage the triplet loss as a metric to learn the feature representations [5–7].

Basically, the triplet loss tries to pull the learned features from the same identity closer and push away features from different identities. Compared with softmax loss, triplet loss directly controls the learning process in embedding space, which ensures features of the same identity are closer than others by a threshold margin. In this way, triplet loss can learn more differences in details than softmax cross-entropy loss. However, triplet loss applications in ReID nowadays are prone to overfitting because of the lack of enough samples in the ReID datasets and the imbalance of samples for different identities. Several studies [8–11] synthesize training images with Generative Adversarial Nets (GAN) [12] to increase the size of the training set, in order to improve the generalization capability of the model. Though the GAN approach is helpful for data augmentation, it also indicates much more effort to generate the samples, which might not be accessible in certain cases, especially when there are too many identities. Guo *et al.* [13] proposed feature normalization to overcome the data imbalance. However, normalization will lead to performance degradation, which is also observed as reported in TriNet [14].

ReID datasets are usually captured by multi-cameras. Thus the inherent changing lights and perspectives will lead to inevitable camera-cased gaps in ReID datasets, indicating very noisy samples. To alleviate the gaps, Zhong *et al.* [15] takes advantage of GAN to transfer images from one camera to another, and Wei *et al.* [16] from one dataset to another. Both these two methods need to spend a lot of time on image generation. Therefore, it is necessary to learn a more robust feature extractor to avoid expensive data augmentation process.

To address these challenges, this paper proposes READNET, a **ReID** oriented **adversarial camera Network** (ACN) with angular triplet loss (ATL). The new loss function, ATL, takes *angle-distance* as the distance metric with a linear angular margin on it. Because angle-distance is not affected by the feature length, feature normalization is still applicable. More importantly, due to the linear angular margin in the embedding space, a linear decision boundary can be guaranteed without performance degradation compared to existing methods. The ACN is designed to address the problem of the camera-cased gaps. ACN consists of a feature extractor and a camera discriminator, and they play a minimax game: the camera discriminator tries to identify which camera the extracted feature was taken from, while the feature extractor tries to extract features without camera information to fight against the discriminator. In this way, it is possible to learn a pedestrian-discriminative-sensitive and multi-camera-invariant feature extractor.

Both ATL and ACN algorithms are straightforward and efficient, and they could be deployed independently or simultaneously. The prototype of READNET is implemented with PyTorch [17] and is evaluated against three widely adopted ReID datasets. The experimental results show that either ATL or ACN outper-

forms the baseline as well as many existing methods, while the combo of them delivers the best results for most test cases in terms of prediction accuracy.

The main contributions of the paper are as follows:

- We propose ATL to leverage “angle-distance” in contrast to the typical triplet loss to ensure a linear decision boundary to address the data imbalance problem due to limited samples.
- We propose ACN to filter the camera information, ensuring the feature extractor can concentrate on the pedestrian information to bridge the gaps stemming from camera noises.

## 2 Related Work

This section discusses how READNET, specifically ATL and ACN, relates to state-of-the-art deep learning based ReID research.

### 2.1 Triplet loss and its Variants

FaceNet [18] proposes the triplet loss for face recognition and clustering, and the results are promising. A potential issue with triplet loss is the difficulty on convergence, and lots of new sampling strategies are introduced to solve this problem. For example, Song *et al.* [19] take all pairwise distances in a batch to take full advantage of a batch. Chen *et al.* [5] adopte quadruplet loss with two negative samples for better generalization capability. Hermans *et al.* [14] propose TriNet with *PK*-style sampling method and hardest example mining, which proved to have no convergence problem on most ReID datasets. TriNet also provides a soft-margin method to pull samples from the same class as close as possible. Ristani *et al.* [20] claim that most hard example mining methods only consider the hardest triplets or semi-hard triplets, but it can be beneficial to take easy triplets as well. They propose adaptive weights triplet loss that provides high and low weights for hard and easy triplets, respectively.

### 2.2 Angular Margin-based Softmax

As the most widely used loss function, softmax loss can be formulated as in Equation (1):

$$\mathcal{L} = -\frac{1}{N} \sum_{i=1}^N \log \frac{e^{W_{y_i}^T x_i + b_{y_i}}}{\sum_{j=1}^n e^{W_{y_j}^T x_i + b_{y_j}}}, \quad (1)$$

where  $x_i \in \mathbb{R}^d$  denotes the feature of  $i$ -th sample with label  $y_i$ ,  $W_j \in \mathbb{R}^n$  is the  $j$ -th column of weight  $W \in \mathbb{R}^{d \times n}$  and  $b_j \in \mathbb{R}^n$  the bias term [21]. SphereFace [22] proposes the angular softmax (A-Softmax) loss that enables convolutional neural networks(CNN) to learn angularly discriminative features by reformulating

$W_j x = \|W_j\| \|x\| \cos\theta_j$ . If we normalize the  $W$  to 1, normalize  $x$  to  $s$ , and multiply an angular margin  $m$ , the softmax loss can be modified to Equation (2):

$$\mathcal{L}_{sph} = -\frac{1}{N} \sum_{i=1}^N \log \frac{e^{s(\cos(m\theta_{y_i}))}}{e^{s(\cos(m\theta_{y_i}))} + \sum_{j \neq y_i} e^{s(\cos(\theta_j))}}. \quad (2)$$

Lots of new angular-based softmax loss functions are proposed based on A-Softmax. For example, CosFace [23] introduces Equation (3):

$$\mathcal{L}_{cos} = -\frac{1}{N} \sum_{i=1}^N \log \frac{e^{s(\cos(\theta_{y_i})-m)}}{e^{s(\cos(\theta_{y_i})-m)} + \sum_{j \neq y_i} e^{s(\cos(\theta_j))}}. \quad (3)$$

And, ArcFace [21] devises a similar loss as in Equation (4):

$$\mathcal{L}_{arc} = -\frac{1}{N} \sum_{i=1}^N \log \frac{e^{s(\cos(\theta_{y_i}+m))}}{e^{s(\cos(\theta_{y_i}+m))} + \sum_{j \neq y_i} e^{s(\cos(\theta_j))}}. \quad (4)$$

The most significant difference between the three angular-based softmax loss functions is the position of margin  $m$ . Although the margins look very similar across these equations, different types of the margin can produce totally different geometric attributes, because the margin has the exact correspondence to the geodesic distance. Though geodesic distance does not makes too much sense for ReID, Equation (4) inspires the design of our angular triplet loss (ATL), in which ReID related issues are took into consideration.

### 2.3 ReID with GAN

Generative Adversarial Nets (GAN) [12] is known as one of the most popular networks in deep learning. One dilemma of ReID is the lack of training data, while GAN can inherently be useful to generate samples. According to our knowledge, Zheng *et al.* [9] is the first ReID related research using GAN to generate random unlabeled samples, and label smoothing is used as there are no labels for synthesized images. Since person re-identification suffers from image style variations caused by multi-cameras, Zhong *et al.* [15] use CycleGAN [24] to transfer images from one camera to another to bridge the gaps. Wei *et al.* [16] propose a Person Transfer Generative Adversarial Network which transfers images from a dataset to another, to bridge the domain gap in different datasets. Additionally, GAN is also used for synthesizing training images to reduce the impact of pose variation [8, 10]. Chen *et al.* [11] propose CR-GAN for synthesizing person images in the unlabeled target domain. READNET not only avoids the generation of additional samples, but also bridges the camera-cased gaps by removing camera-cased information using an adversarial network.

### 3 Methodology

READNET consists of two independent parts: the angular triplet loss function (ATL) and an adversarial camera network (ACN). This section will first look back at triplet loss and then present the design and algorithms of ATL and ACN.

#### 3.1 Triplet Loss

Triplet loss [18] is one of the most popular loss functions of metric learning. For a triplet  $(a, p, n)$ , triplet loss is formulated as Equation (5):

$$\mathcal{L}_{ori} = [D(f_{\theta}(a), f_{\theta}(p)) - D(f_{\theta}(a), f_{\theta}(n)) + m]_{+}, \quad (5)$$

where  $D(x, y)$  is a metric function measuring distance or similarity between  $x$  and  $y$  in the embedding space  $\mathbb{R}^d$ ,  $a$  the anchor sample,  $p$  a positive sample with the same ID as  $a$ , while  $n$  denotes a negative sample.  $f_{\theta}$  is the feature extractor with parameter  $\theta$ . For the sake of clarity,  $(x, y)$  will be used as a shortcut of  $(f_{\theta}(x), f_{\theta}(y))$ , where  $f_{\theta}$  is omitted.  $m$  the margin threshold that  $D(a, p)$  must be less than  $D(a, n)$  by at least  $m$ . The notation  $[\cdot]_{+}$  means  $\max(0, \cdot)$ .

The batch-hard method with  $PK$ -style sampling in TriNet [14] picks  $P$  class randomly, and then samples  $K$  images for each class randomly to create  $P \times K$  anchors in a mini-batch. Then, it chooses one hardest positive and one hardest negative for each anchor to form  $PK$  triplet terms contributing to the triplet loss in a mini-batch.

Triplet loss is designed to pull the positives closer and simultaneously push the negatives away with a threshold margin, aimed at  $D(a, p) + m \leq D(a, n)$ . Many ReID research [5, 18, 20, 25, 26] trains the model with triplet loss taking  $L2$ -norm distance as the distance metric function. However, they suffer from the issues mentioned in Section 3.2.

#### 3.2 Angular Triplet Loss

The essential challenge of ReID is encoding images into robust discriminative features. Though feature normalization is straightforward to alleviate the data imbalance in ReID datasets to some extent [13], it is harmful to the performance, because the normalization operation in Euclidean distance loses some information which can be captured by  $L2$ -norm of features. This is the inspiration and motivation of ATL. After normalization, the Euclidean distance is equivalent to cosine-similarity, so by using cosine-similarity as the metric function, the triplet loss could be formulated as Equation (6):

$$\mathcal{L}_1 = [\cos(\theta_{an}) - \cos(\theta_{ap}) + m]_{+}, \quad (6)$$

where  $\theta_{ap}$  and  $\theta_{an}$  are the angles between  $(a, p)$  and  $(a, n)$ , respectively.

Like ArcFace [21], we transform the cosine-similarity triplet loss to  $\mathcal{L}_2$  as in Equation (7).  $\mathcal{L}_2$  is very different from  $\mathcal{L}_1$  because  $\mathcal{L}_2$  has a linear angular

margin, which could result in a linear decision boundary. Unfortunately,  $\mathcal{L}_2$  might be difficult to converge due to the small gradients, especially when  $m$  is small. Both  $\theta_{ap}$  and  $\theta_{an}$  become 0 very quickly in the experiments, which makes the model hard to optimize.

$$\mathcal{L}_2 = [\cos(\theta_{an}) - \cos(\theta_{ap} + m)]_+. \quad (7)$$

Actually, by leveraging  $\arccos(\cos(\theta)) = \theta$ , the expression  $-\cos(\theta)$  could be eliminated to ensure  $\theta_{ap} + m \leq \theta_{an}$  and avoid the potential convergence issue eventually. Note that  $d(\arccos(x)) = -1/(\sqrt{1-x^2})dx$ , then  $\cos\theta$  is truncated from  $\epsilon - 1$  to  $1 - \epsilon$  to avoid the denominator to be 0. Since  $\epsilon$  is a very small, it is reasonable to set  $\epsilon = 10^{-7}$  in the experiments. Therefore, the triplet loss (embedding loss) with angular margin becomes Equation (8).

$$\mathcal{L}_{emb} = [\theta_{ap} - \theta_{an} + m]_+. \quad (8)$$

As ATL only considers the relative distance but not absolute distance, we add a regularization term  $\mathcal{L}_{reg}$  to limit the norm of features, making the features gather in the embedding space. Finally, the ATL is shown in Equation (9):

$$\mathcal{L}_{atl} = \mathcal{L}_{emb} + w_1 \cdot \mathcal{L}_{reg}, \quad (9)$$

$$\mathcal{L}_{reg} = \frac{1}{3} \sum_{x \in a, p, n} \|x\|_2, \quad (10)$$

where the hyper-parameter  $w_1$  controls the weight of  $\mathcal{L}_{reg}$ . Figure 1 illustrates how ATL  $\mathcal{L}_{atl}$  behaves differently from the original triplet loss  $\mathcal{L}_{ori}$ . Figure 1(a) and Figure 1(b) illustrate the feature distributions learned by the original triplet loss and the angular triplet loss on the testing set, respectively. Unsurprisingly, the results show that the features of same class are clustered according to angles with ATL while the original triplet loss clusters features by  $L_2$ -distance. More importantly, ATL learns wider linear decision boundaries than the original loss.

### 3.3 Adversarial Camera Network

As demonstrated in Section 1, ReID images are usually taken by multi-cameras, causing differences in perspectives, surrounding and poses, making it hard to learn a robust model. The camera related noisy information is also encoded into the extracted features, which is harmful for identifying person-ID. Therefore, the challenge is how to get rid of such camera information from feature representations. This is possible to accomplish by an adversarial network with a camera discriminator.

As illustrated in Figure 2, we define a feature extractor  $F$  with parameter  $\theta_F$  and a camera discriminator  $D$  with parameter  $\theta_D$ . The responsibility of  $F$  is representation learning, namely, extracting perspective-invariant and distinguishable features representations.  $D$  acts like the discriminator in GAN [12], trying to distinguish the camera-ID. The sole goal of  $D$  is to lead the learning process of  $F$  to extract perspective-invariant features representations. Label

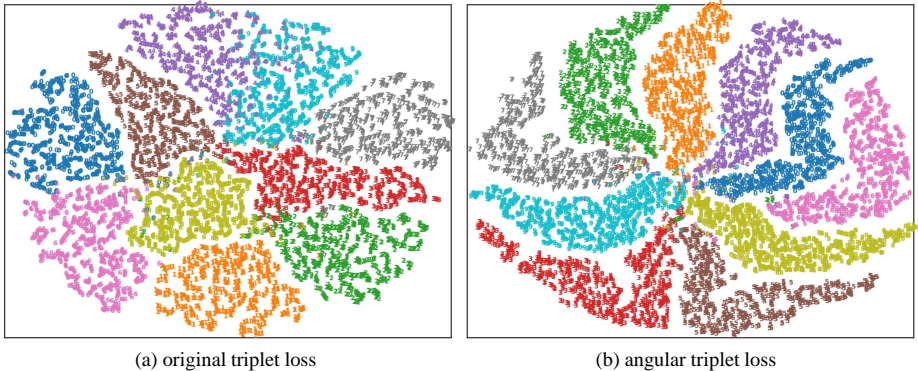


**Fig. 1.** The classification results of  $\mathcal{L}_{ori}$  and  $\mathcal{L}_{atl}$  on the testing set of MNIST [27] with ResNet18 [28]. Since the dataset is relatively simple, the triplet loss here is implemented without hard example mining for demonstration.

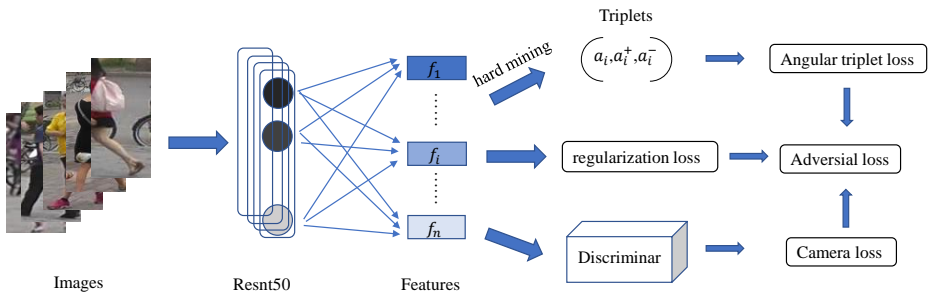


**Fig. 2.** An illustration of the proposed adversarial camera network (ACN) architecture. Given images, fully-connected-layer-removed ResNet50 [28] is employed to extract the features, followed by hard example mining triplets selection, and then ATL is calculated. Extracted features will be discriminated by the camera discriminator for the camera loss. Finally, adversarial loss is formed by combining ATL and camera loss.

smoothing cross entropy [29] is employed for camera-ID prediction. Equation (11) depicts the loss for one sample by ignoring the triplet sampling strategy.

$$\mathcal{L}_{cam} = \sum_{k=1}^K -[y_k^{LS} \log(p_k)], \quad (11)$$

$$y_k^{LS} = y_k(1 - \alpha) + \frac{\alpha}{K}. \quad (12)$$

where  $K$  is the the number of classes, i.e. the number of cameras in a ReID dataset,  $p_k$  is the prediction probability of the  $k$ -th class,  $y_k$  is the indicator variable, and  $y_k$  is 1 when the prediction is correct otherwise 0.  $y_k^{LS}$  is the smooth label of  $y_k$ , with a hyperparameter  $\alpha$ .

**Algorithm 1** The Pseudo-code of the optimization

---

**Initialization:** anchors for current batch:  $\mathcal{A} = \{a_1, \dots, a_m\}$ ;  
 extracted features for current batch:  $\mathcal{T} = \{t_1, \dots, t_m\}$ ;  
 labels and person labels:  $\mathcal{Y} = \{y_{c1}, \dots, y_{cm}\}, \{y_{p1}, \dots, y_{pm}\}$ ;  
 hyperparameters:  $\lambda, \mu, k, w_1, w_2$ ;

1: **repeat**2:   **for**  $k$  steps **do**3:     update parameter  $\theta_D$  by stochastic gradients:

4:

$$\theta_D \leftarrow \theta_D - \mu \cdot \nabla \theta_D \frac{1}{m} \mathcal{L}_{cam}$$

5:   **end for**6:   compose  $m$  triplets by selecting the hardest positive and negative pairs7:   update parameter  $\theta_F$  by descending stochastic gradients:

8:

$$\theta_F \leftarrow \theta_F - \lambda \cdot \nabla \theta_F \frac{1}{m} (\mathcal{L}_{atl} - w_2 \mathcal{L}_{cam})$$

9: **until** convergence**Output:** learned features representations:  $f_{\mathcal{T}}(\mathcal{T})$ 

In real-world applications, the input of  $D$  is the output of  $F$ ,  $F$  is much more deeper than  $D$ , and  $F$  is often trained in advance while  $D$  is not, so it's difficult for  $D$  to fight against. A hyper-parameter,  $w_2$ , is introduced to reduce the weight of  $\mathcal{L}_{cam}$  to make the game between  $D$  and  $F$  more balanced. The final adversarial loss  $\mathcal{L}_{acn}$  is a combination of the  $\mathcal{L}_{atl}$  and  $\mathcal{L}_{cam}$ , as shown in Equation (13):

$$\mathcal{L}_{acn} = \mathcal{L}_{atl} - w_2 \cdot \mathcal{L}_{cam} \quad (13)$$

$$= \mathcal{L}_{emb} + w_1 \cdot \mathcal{L}_{reg} - w_2 \mathcal{L}_{cam}. \quad (14)$$

**Optimization** As shown in the formula  $\mathcal{L}_{acn}$ , the process of feature extractor training is to minimize the triplet loss  $\mathcal{L}_{atl}$  and maximize camera discriminator loss  $\mathcal{L}_{cam}$  at the same time. The camera discriminator learns to distinguish cameras by minimizing  $\mathcal{L}_{cam}$ , which forms an adversarial relationship to the feature extractor as in Equation (15).

$$\tilde{\theta}_F = \arg \min_{\theta_F} (\mathcal{L}_{atl}(\theta_F) - w_2 \mathcal{L}_{cam}(\theta_F, \tilde{\theta}_D)), \quad (15)$$

$$\tilde{\theta}_D = \arg \min_{\theta_D} (\mathcal{L}_{cam}(\tilde{\theta}_F, \theta_D)). \quad (16)$$

Since the goals of the two objective functions are opposite, the training process of the minimax game can be divided into two sub-processes. One sub-process optimizes  $F$ , and the other optimizes  $D$ . Both the two sub-process can be implemented with Adam [30]. In our experiments, we train  $F$  for 1 step after  $k$  steps for the discriminator, as shown in Algorithm 1.



**Table 1.** The overview of the datasets

Datasets	ID	Box	Box/ID	Cam
Market1501	1,501	32,688	21.78	6
DukeMTMC-ReID	1,404	36,411	25.93	8
CUHK03(labeled)	1,467	14,096	9.61	10

## 4 Experiments

Due to the flexible design of READNET, ATL and ACN could be deployed independently, so this section discusses the evaluation results of ATL, ACN as well as the combination of ATL+ACN.

### 4.1 Datasets

READNET is evaluated against 3 widely used ReID datasets: Market1501 [31], DukeMTMC-ReID [32] and CUHK03 [33], in which the first 2 datasets are large and the last one is relatively small. The number of cameras varies across different datasets. Table 1 presents the details of the datasets.

**Market1501** contains 32,688 images of 1,501 person identities, captured by 6 cameras (5 high-resolution cameras, and 1 low-resolution camera). There are 751 identities for training and 750 for testing, 19,732 gallery images and 12,936 training images detected by DPM [34], and 3,368 manually cropped query images.

**DukeMTMC-ReID** consists of 1,404 identities captured by 8 cameras. All the 36,411 bounding boxes are manually labeled. The evaluation protocol in Zheng *et al.* [32] is adopted in our experiments, 16,522 images of 702 identities in the training set, 700 identities in the testing set, with 17,661 images in the gallery and 2,228 images for query.

**CUHK03** is another dataset captured by 5 pairs cameras, including 1,467 identities, and each identity is observed by two disjoint camera views. The bounding boxes are detected in two ways: manually cropped (labeled) and DPM-detected (detected). We focus on the results of the labeled ones, but also report the results of the detected ones. The training and testing protocol for CUHK03 following Zhong *et al.* [35] is adopted in our experiments. For the labeled ones, there are 767 identities with 7,368 images in the training set, and 700 identities in the testing set with 1,400 images for query and 5,328 images for gallery. For the detected ones, 767 identities with 7,365 images are in the training set, and 700 identities in the testing set with 1,400 images for query and 5,332 images for gallery.

### 4.2 Implementation

All experiments share the same global configuration except the margin  $m$  and the camera loss weight  $w_2$ . The prototype is implemented with Pytorch, and all of the models are trained using a single NVIDIA TITAN Xp.

**Training Parameters** *PK*-style batches is employed in the experiments. For reasonable comparison, the batch size is set to 128 to match TriNet [14] by setting  $P$  to 32 and  $K$  to 4, thus a batch contains 32 identities and 4 images for each identity. All images are resized to (128, 64) and we only use random horizontal flips for data augmentation, with the flips probability at 50%.

Adam [30] is chosen as the optimizer for both feature extractor and discriminator network, with base learning rate at  $2 \cdot 10^{-4}$  and  $3 \cdot 10^{-4}$ , respectively, with a same weight decay factor of  $5 \cdot 10^{-4}$ . All other hyper-parameters of the optimizers are default in Pytorch. The number of epochs is set to 600, and the learning rate will decay at 200 epochs and 400 epochs with a decay factor of 0.1.

Features are normalized when computing  $\mathcal{L}_{atl}$  and  $\mathcal{L}_{cam}$ , but not normalized for  $\mathcal{L}_{reg}$  and original triplet loss  $\mathcal{L}_{ori}$ . It is observed that Euclidean-margin can reach its best performance at 0.8, so the Euclidean-margin is set to 0.8 in all the experiments. The angular-margin is set to 0.05 on DukeMTMC-ReID, while 0.08 for the other two datasets when the best accuracy is reached. In addition, the weight  $w_1$  is set at  $10^{-3}$  in loss  $\mathcal{L}_{acn}$  in all experiments. Because the dimensions are different, the weight  $w_2$  is set at  $5 \cdot 10^{-4}$  and  $10^{-4}$  for Euclidean-distance-based triplet loss and ATL, respectively.

**Network Architecture** The baseline is a reimplementaion of TriNet according to the implementation description [14], where pretrained ResNet-50 is used as the feature extractor with the weights provided by He *et al.* [28]. The baseline is abbreviated as *Basel*. The camera discriminator contains 2 fully-connected layers, and ReLU [36] and Dropout [37] are applied after each layer. The output channels for the 2 layers are set at 256 and  $n$ , respectively, where  $n$  is the number of cameras.

**Training Strategy**  $D$  and  $F$  are trained alternately, that is,  $k$  is assigned to 1 in Algorithm 1. As a result, on Market1501, there are approximately 7,000 iterations ( $1501/32 \times 600/2$ ) for feature extractor, and another 7,000 iterations for the discriminator, resulting in a total of 14,000 iterations. The calculation of the iteration number also applies to the other datasets. It usually spends 1 hour for feature extractor training and another 1 hour for camera discriminator training in our configuration.

### 4.3 Evaluation

Mean average precision (mAP) score and cumulative matching curve (CMC) are basic evaluation metrics commonly used in lots of related research [5, 14, 35, 38]. Since ReID is usually regarded as a ranking problem, CMC at rank-1 is reported along with mAP score to make the result more convincing. Single query mode is used in all the experiments.

**Comparison with Baseline** The results illustrated in Table 2 show improvement over baseline for either ATL or ACN in most cases, while ATL+ACN beats

**Table 2.** Comparison on Market1501, DukeMTMC-ReID and CUHK03 with baseline.

Methods	Market1501		DukeMTMC-ReID		CUHK03(labeled)	
	mAP	rank-1	mAP	rank-1	mAP	rank-1
Basel	71.03	86.31	61.28	77.53	53.80	57.14
ATL	73.21	87.50	63.17	79.08	54.57	57.07
ACN	71.37	86.16	61.47	77.56	54.28	56.93
ATL+ACN	<b>74.05</b>	<b>88.78</b>	<b>63.50</b>	<b>79.26</b>	<b>57.20</b>	<b>60.00</b>

the others in all cases. Particularly, ATL+ACN increases mAP from 61.28% to 63.50%, and rank-1 accuracy from 77.53% to 79.26% on DukeMTMC-ReID. In the meantime, ATL+ACN delivers 3.40% and 2.86% improvement in mAP and rank-1 accuracy, respectively on CUHK03 (labeled), and gains 3.02% and 2.47% improvement in mAP and rank-1 accuracy on Market1501, respectively. This indicates that READNET consolidates the benefits of ATL and ACN.

**Comparison with Existing Methods** Table 3 presents the results of READNET and well-known existing methods on CUHK03. As CUHK03 contains the least training images compared with Market1501 and DukeMTMC-ReID, it’s regarded to be the hardest to learn a robust deep representation. However, the results indicate that ATL and ACN can work very well on CUHK03, and again, the combo ATL+ACN is the best for most cases by surpassing many existing methods with 57.20% in mAP and 60.00% in rank-1 accuracy on CHUK03 (labeled).

**Table 3.** Comparison among various methods with our proposed method on CUHK03.

Methods	CUHK03 (labeled)		CUHK03 (detected)	
	mAP	rank-1	mAP	rank-1
PAN [39]	35.0	36.9	34.0	36.3
K-rank+XQ [35]	38.1	40.3	34.7	37.4
DPFL [40]	40.5	43.0	37.0	40.7
SVDNet [41]	-	-	37.3	41.5
Pose-T [10]	42.00	45.10	38.7	41.6
SVDNet+Era [42]	-	-	43.5	48.7
TriNet+Era [42]	53.8	58.1	50.7	<b>55.5</b>
ATL	54.57	57.07	51.03	53.43
ACN	54.28	56.93	51.07	53.57
ATL+ACN	<b>57.20</b>	<b>60.00</b>	<b>51.48</b>	55.36

The results on Market1501 and DukeMTMC-ReID are reported in Table 4. Particularly, ATL itself outperforms many current methods with 63.17% in mAP

**Table 4.** Comparison with various current methods on Market1501 and DukeMTMC-ReID. The first and second best results are illustrated in red and blue, respectively. Best viewed in colors.

Methods	Market1501		DukeMTMC-ReID	
	mAP	rank-1	mAP	rank-1
CAN [43]	35.9	60.3	-	-
LSRO [32]	56.23	78.06	47.13	67.68
MSCAN [3]	57.53	80.31	-	-
SVDNet [41]	62.10	82.30	56.80	76.70
K-rank [35]	63.63	77.11	-	-
PAN [39]	63.35	82.81	51.51	71.59
CamStyle [15]	68.72	88.12	53.48	75.27
Pose-T [10]	68.92	87.65	56.91	78.52
TriNet [14]	69.14	84.92	-	-
TriNet+Era [42]	-	-	56.6	73.0
SVDNet+Era [42]	-	-	62.4	79.3
PL-Net [44]	69.3	88.2	-	-
DPFL [40]	72.6	88.6	60.6	79.2
Aligned [45]	72.80	89.20	-	-
Pose-N [8]	72.58	89.43	53.20	73.58
MLFN [46]	74.30	90.00	62.80	81.20
ATL	73.21	87.50	63.17	79.08
ACN	71.37	86.16	61.47	77.56
ATL+ACN	74.05	88.78	63.50	79.26

and 79.08% in rank-1 accuracy on DukeMTMC-ReID. ATL+ACN achieves competitive metrics with 74.05% in mAP and 88.78% in rank-1 accuracy on Market1501. This means that ACN contributes less than ATL in these datasets.

It can be observed that READNET outperforms some new methods such as Liu *et al.* [10], Qian *et al.* [8] and Yao *et al.* [44] published in the past 2 years. On all the three datasets, both ATL and ACN can achieve competitive performance, while ATL+ACN usually reaches the highest scores, which is a strong implication that both ATL and ACN are helpful to learn pedestrian-discriminative-sensitive and multi-camera-invariant representations and the combination of them READNET could leverage them simultaneously.

**Comparison of Various Margins** As an important hyper-parameter in triplet loss, the variation of margin can affect the results significantly, so it is necessary to evaluate how this is related. Since ACN has nothing to do with the margin, experiments are only conducted with ATL for fair comparison. The margin for the baseline is  $\{0.2, 0.5, 0.8, 1.0\}$ , and  $\{0.02, 0.05, 0.08, 0.1\}$  for ATL. Table 5 shows the results in details. Apparently, ATL outperforms Euclidean-distance-based triplet loss in all metrics.

**Table 5.** Comparison of various margins. The first and second best results are highlighted in red and blue respectively. Best viewed in colors.

Method(m)	Market1501		DukeMTMC		CUHK03(labeled)	
	mAP	rank-1	mAP	rank-1	mAP	rank-1
Basel(0.2)	70.29	86.10	59.56	76.26	51.82	54.71
Basel(0.5)	70.55	86.28	60.90	77.78	53.57	55.93
Basel(0.8)	71.03	86.31	61.28	77.53	53.8	57.14
Basel(1.0)	71.51	84.86	60.82	77.06	53.8	56.57
ATL(0.02)	70.89	86.61	62.57	78.55	51.55	54.50
ATL(0.05)	71.97	87.41	63.17	79.08	53.08	55.14
ATL(0.08)	73.21	87.50	59.53	76.80	54.57	57.07
ATL(0.1)	69.81	85.36	58.17	75.99	55.45	58.43

## 5 Conclusions

To address the data imbalance and domain gap challenges in ReID applications, this paper proposed READNET, an adversarial camera network with an angular triplet loss. The ATL function performs beyond the Euclidean-distance-based triplet loss functions on various datasets to mitigate the effect of data limitation as well as data imbalance. For the domain gaps introduced by independent cameras, the adversarial camera network is devised to filter useless multi-camera information, which encourages feature extractor to learn pedestrian-discriminative-sensitive and multi-camera-invariant feature representations. The model is more robust to tolerate the noise introduced by cameras. Though ATL and ACN are targeted for ReID initially, they could be ported and implemented in other domain applications, especially triplet loss related or multi-view related use cases. In the future, we will extend our work to address the potential training instability problem in ReID.

## References

1. Chen, B., Deng, W., Hu, J.: Mixed high-order attention network for person re-identification. In: Proceedings of the IEEE International Conference on Computer Vision. (2019) 371–381
2. Sun, Y., Zheng, L., Yang, Y., Tian, Q., Wang, S.: Beyond part models: Person retrieval with refined part pooling (and a strong convolutional baseline). In: Proceedings of the European Conference on Computer Vision (ECCV). (2018) 480–496
3. Li, D., Chen, X., Zhang, Z., Huang, K.: Learning deep context-aware features over body and latent parts for person re-identification. In: Proceedings of the IEEE Conference on Computer Vision and Pattern Recognition. (2017) 384–393
4. Zhao, H., Tian, M., Sun, S., Shao, J., Yan, J., Yi, S., Wang, X., Tang, X.: Spindle net: Person re-identification with human body region guided feature decomposition and fusion. In: Proceedings of the IEEE Conference on Computer Vision and Pattern Recognition. (2017) 1077–1085
5. Chen, W., Chen, X., Zhang, J., Huang, K.: Beyond triplet loss: a deep quadruplet network for person re-identification. In: Proceedings of the IEEE Conference on Computer Vision and Pattern Recognition. (2017) 403–412
6. Cheng, D., Gong, Y., Zhou, S., Wang, J., Zheng, N.: Person re-identification by multi-channel parts-based cnn with improved triplet loss function. In: Proceedings of the IEEE conference on computer vision and pattern recognition. (2016) 1335–1344
7. Xiao, Q., Luo, H., Zhang, C.: Margin sample mining loss: A deep learning based method for person re-identification. arXiv preprint arXiv:1710.00478 (2017)
8. Qian, X., Fu, Y., Xiang, T., Wang, W., Qiu, J., Wu, Y., Jiang, Y.G., Xue, X.: Pose-normalized image generation for person re-identification. In: Proceedings of the European Conference on Computer Vision (ECCV). (2018) 650–667
9. Zheng, Z., Zheng, L., Yang, Y.: Unlabeled samples generated by gan improve the person re-identification baseline in vitro. In: Proceedings of the IEEE International Conference on Computer Vision. (2017)
10. Liu, J., Ni, B., Yan, Y., Zhou, P., Cheng, S., Hu, J.: Pose transferrable person re-identification. In: Proceedings of the IEEE Conference on Computer Vision and Pattern Recognition. (2018) 4099–4108
11. Chen, Y., Zhu, X., Gong, S.: Instance-guided context rendering for cross-domain person re-identification. In: Proceedings of the IEEE International Conference on Computer Vision. (2019) 232–242
12. Goodfellow, I., Pouget-Abadie, J., Mirza, M., Xu, B., Warde-Farley, D., Ozair, S., Courville, A., Bengio, Y.: Generative adversarial nets. In: Advances in neural information processing systems. (2014) 2672–2680
13. Guo, Y., Zhang, L.: One-shot face recognition by promoting underrepresented classes. arXiv preprint arXiv:1707.05574 (2017)
14. Hermans, A., Beyer, L., Leibe, B.: In defense of the triplet loss for person re-identification. arXiv preprint arXiv:1703.07737 (2017)
15. Zhong, Z., Zheng, L., Zheng, Z., Li, S., Yang, Y.: Camera style adaptation for person re-identification. In: The IEEE Conference on Computer Vision and Pattern Recognition (CVPR). (June 2018)
16. Wei, L., Zhang, S., Gao, W., Tian, Q.: Person transfer gan to bridge domain gap for person re-identification. In: Proceedings of the IEEE conference on computer vision and pattern recognition. (2018) 79–88

17. Paszke, A., Gross, S., Chintala, S., Chanan, G., Yang, E., DeVito, Z., Lin, Z., Desmaison, A., Antiga, L., Lerer, A.: Automatic differentiation in pytorch (2017)
18. Schroff, F., Kalenichenko, D., Philbin, J.: Facenet: A unified embedding for face recognition and clustering. In: Proceedings of the IEEE conference on computer vision and pattern recognition. (2015) 815–823
19. Oh Song, H., Xiang, Y., Jegelka, S., Savarese, S.: Deep metric learning via lifted structured feature embedding. In: Proceedings of the IEEE Conference on Computer Vision and Pattern Recognition. (2016) 4004–4012
20. Ristani, E., Tomasi, C.: Features for multi-target multi-camera tracking and re-identification. In: Proceedings of the IEEE conference on computer vision and pattern recognition. (2018) 6036–6046
21. Deng, J., Guo, J., Xue, N., Zafeiriou, S.: Arcface: Additive angular margin loss for deep face recognition. In: Proceedings of the IEEE Conference on Computer Vision and Pattern Recognition. (2019) 4690–4699
22. Liu, W., Wen, Y., Yu, Z., Li, M., Raj, B., Song, L.: Sphereface: Deep hypersphere embedding for face recognition. In: Proceedings of the IEEE conference on computer vision and pattern recognition. (2017) 212–220
23. Wang, H., Wang, Y., Zhou, Z., Ji, X., Gong, D., Zhou, J., Li, Z., Liu, W.: Cosface: Large margin cosine loss for deep face recognition. In: Proceedings of the IEEE Conference on Computer Vision and Pattern Recognition. (2018) 5265–5274
24. Zhu, J.Y., Park, T., Isola, P., Efros, A.A.: Unpaired image-to-image translation using cycle-consistent adversarial networks. In: Proceedings of the IEEE international conference on computer vision. (2017) 2223–2232
25. Ding, S., Lin, L., Wang, G., Chao, H.: Deep feature learning with relative distance comparison for person re-identification. *Pattern Recognition* **48**(10) (2015) 2993–3003
26. Sohn, K.: Improved deep metric learning with multi-class n-pair loss objective. In: Advances in Neural Information Processing Systems. (2016) 1857–1865
27. LeCun, Y., Bottou, L., Bengio, Y., Haffner, P.: Gradient-based learning applied to document recognition. *Proceedings of the IEEE* **86**(11) (1998) 2278–2324
28. He, K., Zhang, X., Ren, S., Sun, J.: Deep residual learning for image recognition. In: Proceedings of the IEEE conference on computer vision and pattern recognition. (2016) 770–778
29. Szegedy, C., Vanhoucke, V., Ioffe, S., Shlens, J., Wojna, Z.: Rethinking the inception architecture for computer vision. In: The IEEE Conference on Computer Vision and Pattern Recognition (CVPR). (June 2016)
30. Kingma, D.P., Ba, J.: Adam: A method for stochastic optimization. arXiv preprint arXiv:1412.6980 (2014)
31. Zheng, L., Shen, L., Tian, L., Wang, S., Wang, J., Tian, Q.: Scalable person re-identification: A benchmark. In: Computer Vision, IEEE International Conference on. (2015)
32. Zheng, Z., Zheng, L., Yang, Y.: Unlabeled samples generated by gan improve the person re-identification baseline in vitro. In: The IEEE International Conference on Computer Vision (ICCV). (Oct 2017)
33. Li, W., Zhao, R., Xiao, T., Wang, X.: Deepreid: Deep filter pairing neural network for person re-identification. In: CVPR. (2014)
34. Felzenszwalb, P., McAllester, D., Ramanan, D.: A discriminatively trained, multi-scale, deformable part model. In: 2008 IEEE Conference on Computer Vision and Pattern Recognition, IEEE (2008) 1–8

35. Zhong, Z., Zheng, L., Cao, D., Li, S.: Re-ranking person re-identification with k-reciprocal encoding. In: Proceedings of the IEEE Conference on Computer Vision and Pattern Recognition. (2017) 1318–1327
36. Glorot, X., Bordes, A., Bengio, Y.: Deep sparse rectifier neural networks. In: Proceedings of the fourteenth international conference on artificial intelligence and statistics. (2011) 315–323
37. Srivastava, N., Hinton, G., Krizhevsky, A., Sutskever, I., Salakhutdinov, R.: Dropout: a simple way to prevent neural networks from overfitting. The journal of machine learning research **15**(1) (2014) 1929–1958
38. Wang, B., Yang, Y., Xu, X., Hanjalic, A., Shen, H.T.: Adversarial cross-modal retrieval. In: Proceedings of the 25th ACM international conference on Multimedia, ACM (2017) 154–162
39. Zheng, Z., Zheng, L., Yang, Y.: Pedestrian alignment network for large-scale person re-identification. IEEE Transactions on Circuits and Systems for Video Technology **29**(10) (2018) 3037–3045
40. Chen, Y., Zhu, X., Gong, S.: Person re-identification by deep learning multi-scale representations. In: Proceedings of the IEEE International Conference on Computer Vision Workshops. (2017) 2590–2600
41. Sun, Y., Zheng, L., Deng, W., Wang, S.: Svdnet for pedestrian retrieval. In: Proceedings of the IEEE International Conference on Computer Vision. (2017) 3800–3808
42. Zhong, Z., Zheng, L., Kang, G., Li, S., Yang, Y.: Random erasing data augmentation. arXiv preprint arXiv:1708.04896 (2017)
43. Liu, H., Feng, J., Qi, M., Jiang, J., Yan, S.: End-to-end comparative attention networks for person re-identification. IEEE Transactions on Image Processing **26**(7) (2017) 3492–3506
44. Yao, H., Zhang, S., Hong, R., Zhang, Y., Xu, C., Tian, Q.: Deep representation learning with part loss for person re-identification. IEEE Transactions on Image Processing **28**(6) (2019) 2860–2871
45. Zhang, X., Luo, H., Fan, X., Xiang, W., Sun, Y., Xiao, Q., Jiang, W., Zhang, C., Sun, J.: Alignedreid: Surpassing human-level performance in person re-identification. arXiv preprint arXiv:1711.08184 (2017)
46. Chang, X., Hospedales, T.M., Xiang, T.: Multi-level factorisation net for person re-identification. In: Proceedings of the IEEE Conference on Computer Vision and Pattern Recognition. (2018) 2109–2118